Supplementary Material (ESI) for Chemical Communications

Size Dependent Oxygen Buffering Capacity of Ceria Nanocrystals

Jiahui Xu[1], Jeffrey Harmer[1], Guoqiang Li[1], Thomas Chapman[1], Paul Collier[2], Sarennah Longworth[2], Shik Chi Tsang*[1]

Electronic Supporting Information

Synthesis

The synthesis method used is based on modified method reported by M. D. Herna′ndez-Alonso, A. B. Hungrı′a, A. Martı′nez-Arias, J. M. Coronado, J. C. Conesa, J. Soria and M. Ferna′ndez-Garcı′a, Phys. Chem. Chem. Phys., 2004, 6, 3524–3529.

One microemulsion containing 5g aqueous phase solutions (0.025 M to 0.5 M) of cerium (III) nitrate hexahydrate (sigma-aldrich) was prepared. 29 g organic solvent (n-Heptane, > 99%, Fisher) was used in an amount such as to yield different water to oil ratios. 19 g Triton® X-100 (Aldrich) and 15g 1-hexanol (> 99%, Aldrich) were utilized as surfactant and co-surfactant, respectively. Another microemulsion, which contained as 5g tetramethylammonium hydroxide pentahydrate (25wt% in water, sigma-aldrich) aqueous phase solutions, with 29g n-Heptane, 19 g Triton® X-100 (Aldrich) and 15g 1-hexanol, was prepared separately. Each microemulsion is stirred for 4 hours to make the mixture totally distributive.

In the second stage, both microemulsions were mixed, and then stirred for 24 hrs. After 24hrs, the liquid was centrifuged, decanted and the resulting precipitate rinsed thoroughly (four times) with ethanol. The solid obtained was first dried at room temperature, then at 353 K for another 24 hrs and finally calcined in air for 2 hrs at 773 K using a 2 K min^{-1} ramp. The final samples will be here after referred to as MCE-x. The samples were kept in nitrogen filled dry box after calcination to reduce contamination of carbonate phase formed from reaction with carbon dioxide from air.

XRD and TEM

Powder XRD patterns (Figure S1) were recorded on a Siemens D5000 high-resolution X-ray powder diffractometer using Cu*K*α radiation. Also, the collected XRD data were analyzed (fluorite structure) and refined by Rietveld method (Figure S3) using data up to 125 ^{o} in 2θ (However, the samples with the sizes 4.9 nm and 4.4 nm showed a higher degree of error in R_{wp} than other samples of error <15%). The particle size and distribution were determined by Scherrer treatments of 3 most intense XRD peaks and TEM with analysis more than 70 particles for each sample.

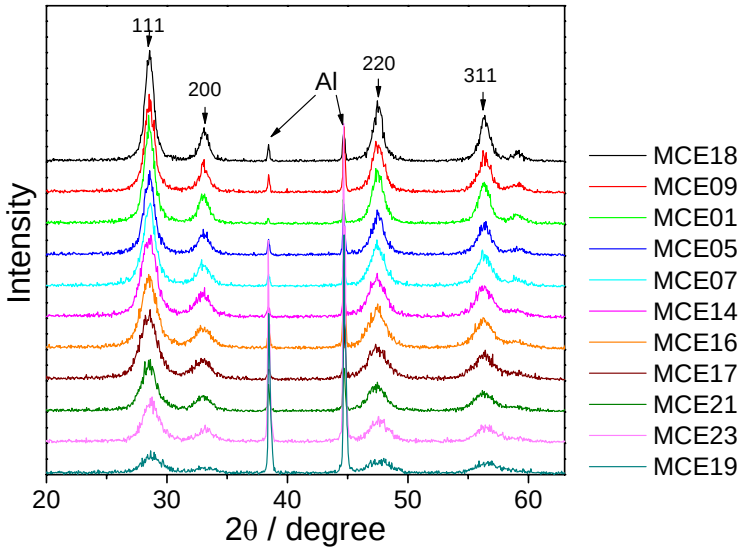

Table S1

Samples	Particle size/nm
MCE18	12.5
MCE09	9.9
MCE01	9.4
MCE05	8.5
MCE07	7.8
MCE14	6.0
MCE16	5.8
MCE17	5.3
MCE21	5.1
MCE23	4.9
MCE19	4.4

Figure S1 *XRD patterns of ceria synthesized by MCE method.*
(The particle size of the ceria is assumed to be the crystallite size calculated using the Scherrer equation over all the peaks.)

TEM analysis was carried out using a JEOL JEM-3000F working at 300 kV. High Resolution Electron Microscopy (HREM) showed the atomic arrangement. The crystal structure was examined by selected area electron diffraction (SAED) patterns (Figure S2) which were recorded by a 1k×1k CCD camera. The lattice constants were then carefully calculated from SAED patterns. In order to achieve this, it is essential to calibrate the experimental patterns with the known diffraction pattern. This was achieved by setting up a protocol of constant lens settings for the microscope, which enabled the calibration against an Au polycrystalline sample to be maintained to a high accuracy. By labeling the Au diffraction rings with the corresponding Au (111), (200), (220) and (311) planes, we obtained the scattering radian per pixel on the CCD screen. This value

was used to calculate the scattering angles for various CeO_2 planes of CeO_2 SAED patterns, and the reciprocal of the scattering angle corresponds to the interplane spacing, from which the lattice constants were deduced. The ring patterns obtained in SAED patterns shown as insets in Figure S2 in the main text of the manuscript confirm the nanocrystallinity and the fluorite structure.

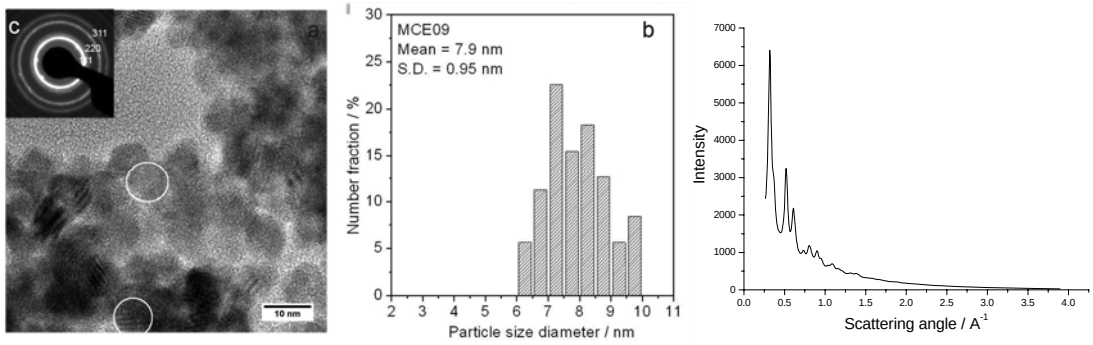

Sample MCE09 with size 9.9 nm determined by XRD; lattice constant= 5.417

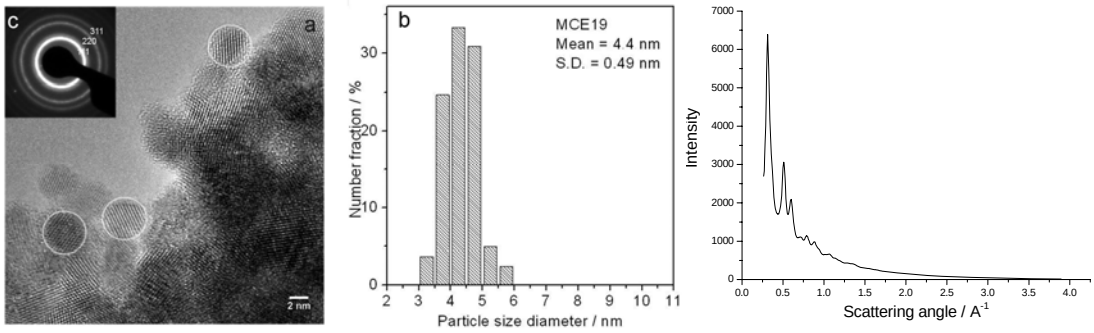

Sample MCE19 with size 4.4 nm determined by XRD; lattice constant= 5.458

Figure S2 *High-resolution electron micrographs of CeO_2 particles synthesized by MCE method.*

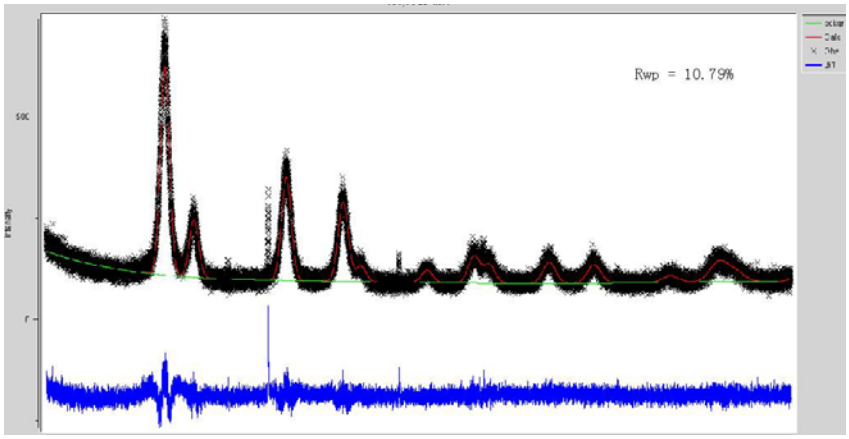

Figure S3 *Experimental XRD patterns calculated through a Rietveld refinement based on the CeO_2 (cubic) structure. The black crosses are the raw data; the red line is the calculated pattern and the blue line below is the difference. (Sample MCE 14, particle size 6.0 nm)*

XPS

X-ray photoelectron spectroscopy (XPS) was performed using ESCA II lab. The samples were analyzed without pretreatment.

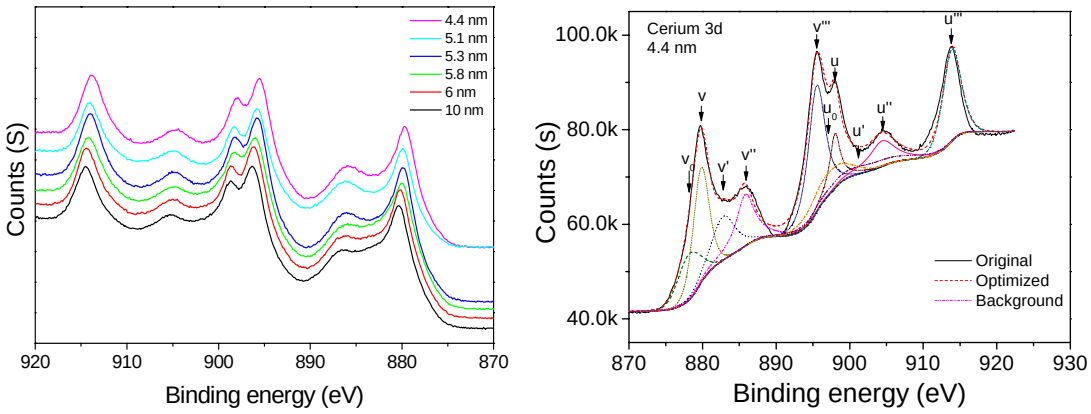

Figure S4 *Left: Cerium 3d photoemission spectra for samples with different particle sizes; Right: The possible individual contributions, peaks denoted by the subscripts v and u are assigned to* $3d_{5/2}$ *and* $3d_{3/2}$ *states respectively.*

In order to investigate the changes in the nanoceria surface chemistry, x-ray photoelectron spectroscopy (XPS, see Figures S4, S5) was performed on the samples under optimized conditions. v_0, v', u_0, and u' peaks are attributed to Ce^{3+}; while v, v'', v''', u, u'', and u''' are characteristic of Ce^{4+}. Similar peak fitting was done for the XPS spectra of ceria nanoparticles with different sizes. The peak positions for all the samples are listed in Table S2.

Table S2 *XPS binding energies of individual peaks of the Ce 3d spectrum for different ceria nanoparticles.*

Particle	Ce^{4+}						Ce^{3+}			
Size / nm	v	v''	v'''	u	u''	u'''	v_0	v'	u_0	u'
10	880.3	886.5	896.2	898.7	905.3	914.5	878.7	883.3	897.6	902
6	880.2	886.4	896.1	898.7	905.3	914.4	878.6	883.3	897.7	902
5.8	880	886.1	895.85	898.4	904.7	914.1	878.5	883.6	897.45	901.6
5.3	879.9	886	895.8	898.2	904.9	914	878.4	883	897.3	901.3
5.0	879.8	885.8	895.5	898	904.4	913.9	878.2	882.8	897.1	901.1
4.4	879.8	885.8	895.5	898	904.4	913.9	878.2	882.8	897.1	901.1

A semiquantitative analysis of the integrated peak area can provide the concentration of Ce^{3+} ions in the synthesized nanoparticles. It can be calculated as:

$$[Ce^{3+}] = \frac{A_{v0} + A_{v'} + A_{u0} + A_{u'}}{A_{v0} + A_{v'} + A_{u0} + A_{u'} + A_{v} + A_{v''} + A_{v'''} + A_{u} + A_{u''} + A_{u'''}}, \quad \text{(Equ. 1)}$$

where A_i is the integrated area of peak "i".

Table S3 *Concentration of Ce^{3+} as a function of nanoceria particle size calculated using above equation. (Refer to Equ. 1)*

Particle size / nm	10	6	5.8	5.3	4.9	4.4
Concentration of Ce^{3+} / %	29.4	28.8	27.9	27.6	27.9	29.5

Similar method is used in O 1s spectrum of ceria.

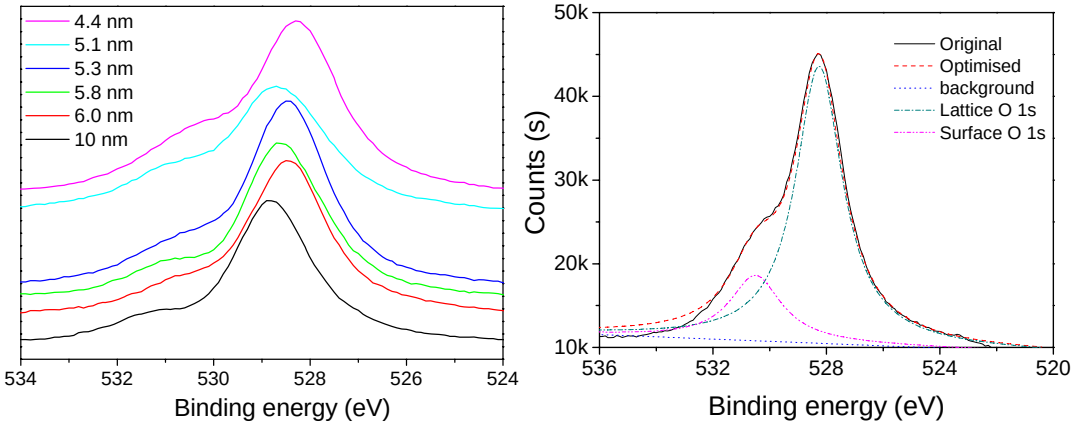

Figure S5 *Left: Oxygen* ***1s*** *photoemission spectra for samples with different particle sizes; Right: Oxygen* ***1s*** *photoemission spectra for the sample with the particle size 4.4 nm. Also shown are the possible individual components (dotted lines) obtained through curve fitting.*

Table S4 *XPS binding energies of individual peaks of the O 1s spectrum for different CeO_2 nanoparticles samples.*

Particle size	Surface oxygen species		Lattice oxygen species	
(nm)	BE (eV)	A_{surf} (%)	BE (eV)	A_{latt} (%)
10	531.3	3.14	528.8	96.86
6	531	7.07	528.5	92.93
5.8	531.13	8.55	528.5	91.45
5.3	531	12.4	528.5	87.6
4.9	530.9	13.7	528.6	86.3
4.4	530.5	20.5	528.3	79.5

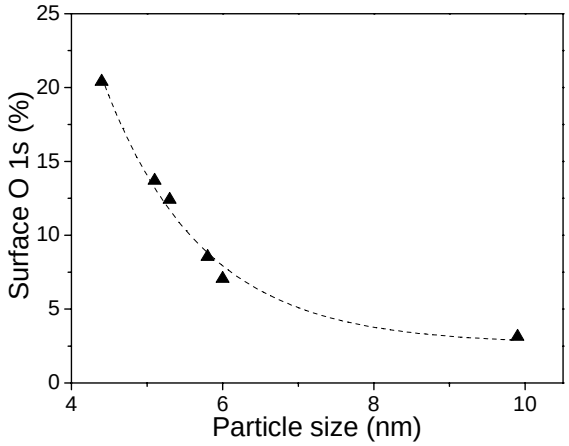

It is interesting to note from the above Table that the decrease in lattice oxygen (528.8 eV) matches with new broad surface oxygen peak at binding energy at 531 eV. The broad peak grows in size and gradually shifted to slight lower binding energy (*ca*. 2eV above lattice oxygen) at the lowest size. This new peak position has been previously observed and there has been debate concerning the exact origin of such peak but it has been consistently ascribed to superoxide species (Dolle, P.; Drissi, S.; Besancon, M.; Joupille, J. Surf. Sci. 1992, 269/270, 687-690.)

Electronic paramagnetic resonance (EPR)

X-band CW EPR spectra (Figure S6a-c) were recorded at room temperature on a Bruker EMX spectrometer using an Elexsys high sensitivity probehead. Cerium oxide samples, without pretreatment, where prepared in 4 mm tubes and weighed carefully to an accuracy of 0.01 mg.

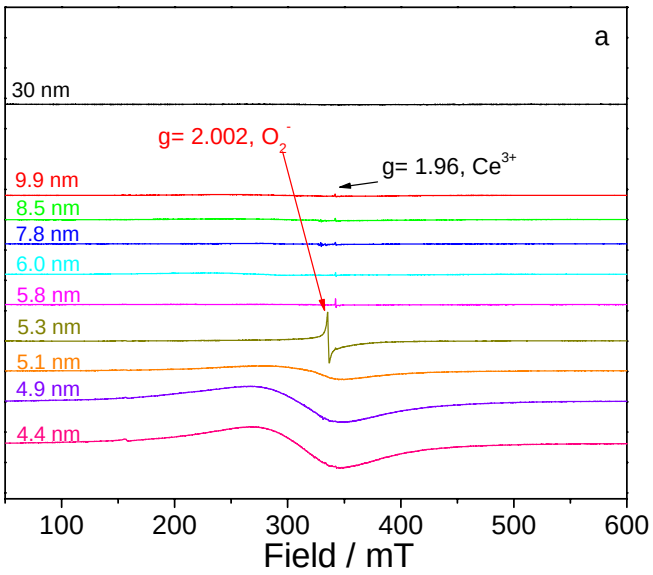

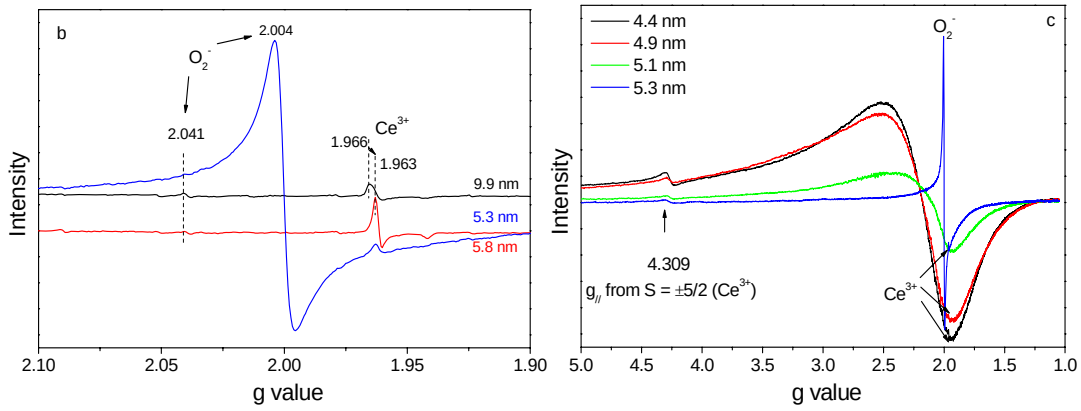

Figure S6a-c: *X-band (9.402 GHz) CW EPR spectra at room temperature of ceria with different particle sizes.*

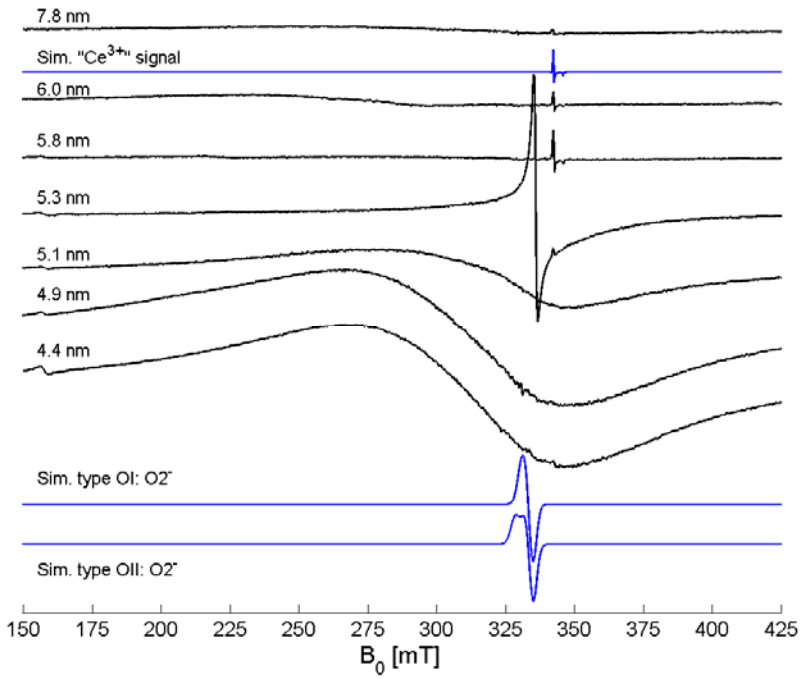

Figure S6d*: EPR spectra of ceria (7.8nm, 6.0nm and 5.8nm were magnified by 5 times) with different particle sizes showing the formation of superoxide surfaces at or below 5.5nm. Blue traces show simulations for the signal usually denoted as "Ce^{3+}" ($g_\perp$ = 1.963, $g_{||}$ = 1.943) and for typical type OI ($g_\perp$ = 2.011, $g_{||}$ = 2.032) and type OII (g_1 = 2.008, g_2 = 2.013, g_3 = 2.047) Ce^{4+}–O_2^- radicals (refer to* the papers from *Oliva, C and Soria J and co-workers, respectively).*

Calculation of the spin number was based on a powder sample of Cu(II)TPP with a molar mass of 677.5 g and 1 spin per molecule. The CW EPR signal intensity *vs* electron spin number was obtained from the double integral of the spectrum. Ceria samples were weighed to an accuracy of 0.01mg. The CW EPR signal intensity of the broaden peak (Figure S6a) from the samples with sizes smaller than 5.1 nm where also calculated from the double integral, enabling the number of spins per gram of ceria to be determined. All calibration measurements were made with a microwave power of 5.02 mW, a modulation amplitude of 2.00 G, and 100 kHz modulation

frequency.

As can be seen from Figure S6b-c, the signals at g~1.96 and g ~ 4.309 previously attributed to Ce^{3+} coupled with conduction electrons on ceria (Oliva, C.; Termignone, G.; Vatti, F. P.; Forni, L.; Vishniakov, A.V. *J. Mater. Sci.* 31 (1996) 6333-6338) are clearly present but are comparatively weak (note that uncoupled Ce^{3+} EPR governed by 4f electrons normally requires temperature below 20K to be visible) and its intensity is approximately constant over the range of particle sizes, a result consistent with the XPS data.

From the above spectra, we also observed a paramagnetic peak that was assigned to a radical with O_2^- character (g = 2.002, linewidth L_{pp}=80 MHz) in the 5.3nm ceria. This signal was clearly observed at room temperature. The nature of this peak is believed to be Ce^{3+} + O_2 giving Ce^{4+} + $(O_2)^-$. We excluded the possibility of this peak arisen from contaminated carbonaceous impurities in the 5.3nm sample since this peak was not as sharp as those of typical carbon radicals (linewidth L_{pp}=80 MHz indicating a species contributed to by electron-electron or spin-orbital interactions) and was not present in the other samples which were prepared using identical procedures. We noted that this signal did not change upon cooling to 77K. The peak was severely broadened (g~2.13 to 2.21, L_{pp}~2800 MHz) and increased significantly in strength at decreasing particle size. Again, there was no apparent change of these spectra in the LNT. We also carried a second TPR run of the 5.1 nm particle size sample after quenching it from the first TPR treatment, the broad EPR signal was totally lost (reduced), giving a small peak of g~2.003 (L_{pp}=3MHz) (assigned to electrons trapped at surface vacancies). This clearly suggests that the peak can be reducible matching with the nature of adsorbed O_2^-.

However, these g-values did not correspond well with the typical values reported due to Ce^{4+}– O_2^- species on bulk ceria in the literature, which are in the range *c.a.* 2.00-2.05. (Oliva, C.; Termignone, G.; Vatti, F. P.; Forni, L.; Vishniakov, A.V. *J. Mater. Sci.* 31 (1996) 6333-6338; Soria J., Martínez-Arias A.; Conesa J.C. *J. Chem. Soc. Faraday Trans.* 91 (1995), 1669-1678). Such reported Ce^{4+}– O_2^- species give a relatively sharp EPR spectrum with anisotropic g_z, g_y and g_x parameters with the g_z depending of the adsorption site charge (please refer to the two reviews by Tench and Che in Advances in Catalysis vol. 31). We have carried out a simulation of the reported OI type and OII type as shown in the Figure S6d below. As noted from their spectra and the reported spectra in literature the typical ^{17}O hyperfine couplings for Ce^{4+}–O_2^- species are <80 MHz in bulk ceria. Our broad linewidths and high g-values collected clearly indicate significant coupling of these species on nano-ceria surface. These features would also limit the peak resolutions even if ^{17}O is employed (reported ^{17}O hyperfine couplings for Ce^{4+}–O_2^- species are in general <80 MHz).

We therefore attribute that the large electron-electron interactions depend on oxygen defect concentration and defect clusters which have been known to inversely depend on particle size (Z.W. Wang, S. Seal, S. Patil, C.S. Zha, Q. Xue, Journal of Physical Chem C. 2007, 111, 11756-11759). There is also a possibility that have a larger spin-orbit interaction due to the Ce 4f orbitals on defective sites on the nanoparticle surface.

TPR

Temperature programmed reduction (TPR) was performed by ramping the temperature at a heating rate of 10 K/min from room temperature 1273K and by using a mixture of 5% H_2/Ar (see Fig. S7).

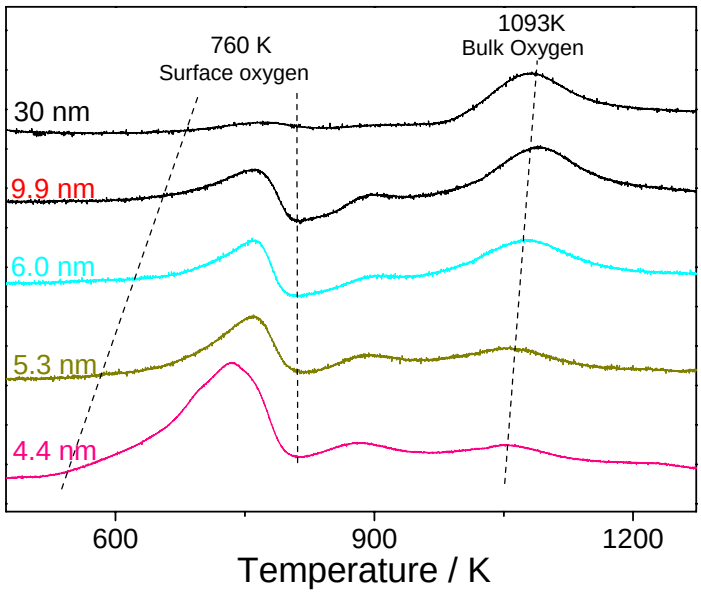

Figure S7 *H_2- Temperature Programmed Reduction (TPR) profiles of nano-ceria with different sizes.*

Reduction signals were recorded using normalized 30 mg ceria sample: the baseline were initially collected and subtracted from the data by the Gaussian method (Figure S8). Based on the calibration using standard sample (CuO), the hydrogen consumption for the reduction of oxygen species from the ceria samples was calculated. Contamination of carbonate phase in the samples is carefully reduced by storing the samples in nitrogen dry box prior the TPR experiments. The TPR reduction of carbonate will give a characteristic peak at 800K (no overlap with the oxygen reduction peaks), which is used to check the sample contamination. All our sample did not give the peak at significant size hence the degree of contamination was very low. As seen from typical TPR graph, the surface oxygen was attributed to the first peak (760 K, A1), the bulk oxygen was assigned to the third peak (1000 K, A3), and the second reduction peak was found to be around 900 K (A2).

The percent of surface oxygen is (A1)/(A1+A2+A3)*100%; the bulk oxygen is A3/(A1+A2+A3)*100%. Results collected from EPR, XPS and TPR (30 mg ceria) are summarized in Table S5.

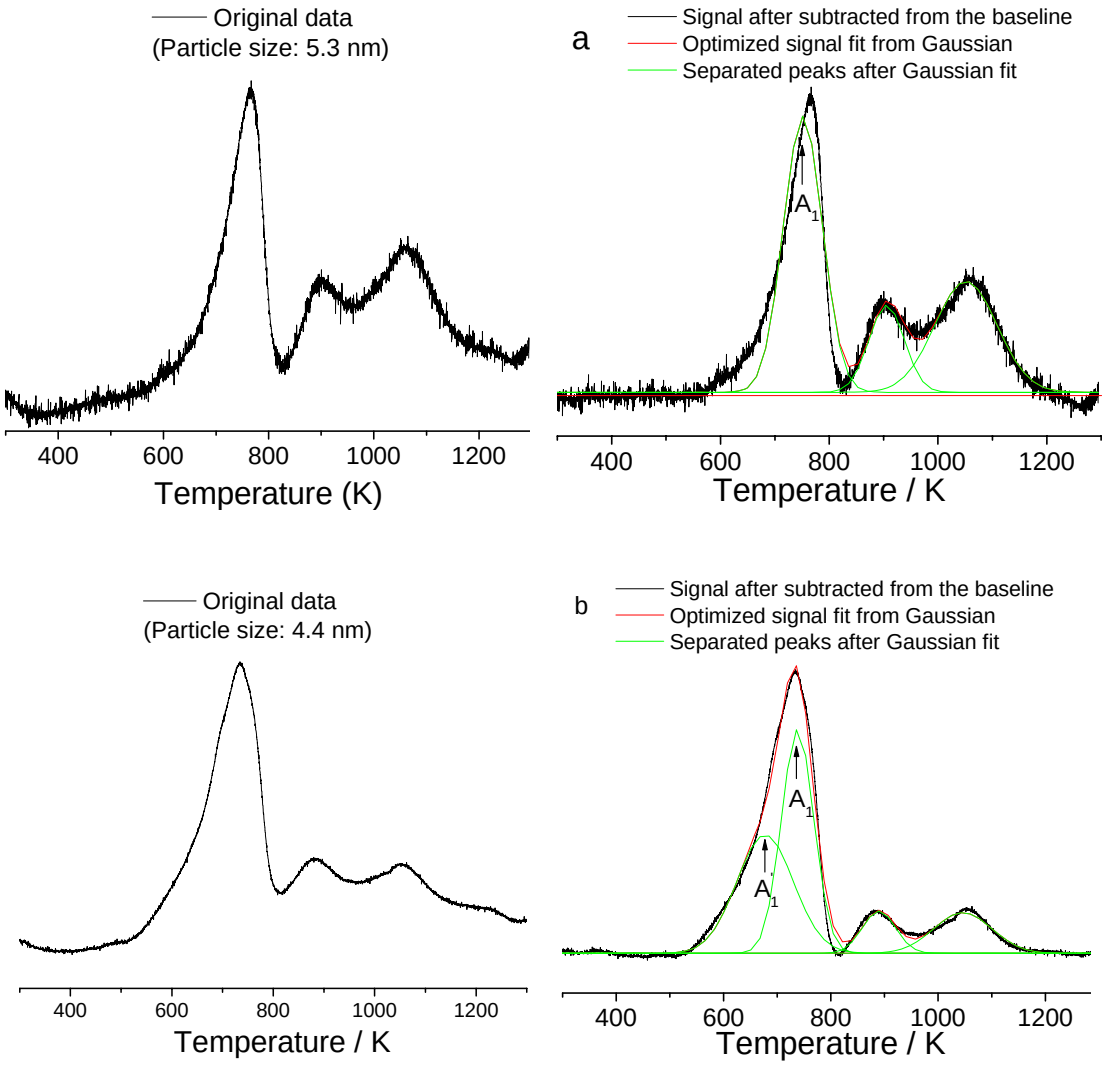

For the sample with the particle size smaller than 5.1 nm, the surface oxygen peak A1 is able to be separated into two peaks the first peak A1' at about 675 K and the second peak A1 was around 750K.

Figure S8 *Gaussian fit H_2-TPR profiles of nano-ceria with different sizes.*

Table S5 [O] *analysis from H_2-TPR and EPR in 30 mg ceria (CeO_{2-x})*

Size (nm)	Concentration of Ce^{3+} from XPS (%)	Oxygen calculated from TPR: Surface $[O]_{surf}$ (μmol)	Surface %	Bulk $[O]_{bulk}$ (μmol)	Bulk %	$[O]_{total}$ (μmol)	$[O_2^-]$ (μmol) EPR
9.9	29.4	8.9	39.90	12.5	56.18	22.3	-
8.5	-	10.5	48.69	10.2	47.43	21.6	-
7.8	-	10.9	50.86	9.8	45.64	21.5	-
6.0	28.8	11.1	51.43	9.4	43.49	21.7	-
5.8	27.9	14.0	64.05	7.4	33.93	21.9	NM
5.3	27.6	14.9	66.85	7.0	31.09	22.4	NM
		$[O]_{A1'}$ 675K	$[O]_{A1}$ 750K	%	%		
5.1	27.9	3.7	14.1	14.1	54.3	6.9	26.74	26.2	3.34
4.9	-	10.5	12.9	34.4	39.0	5.7	17.86	31.9	9.92
4.4	29.5	14.1	15.3	38.6	41.6	5.0	13.52	36.7	10.43

Taking the contribution of thermal dilation into account (for CeO_2 and CeO_{2-x}, this value is about 6.34 x 10^{-5} Å/K, the lattice expansion is commonly interpreted as a consequence of reduction of Ce^{4+} ions to Ce^{3+}, since the radius of the Ce^{3+} ion being larger than of Ce^{4+} (1.14Å vs 0.97Å, according to the data of Shannon and Prewitt)[1]. Undoubtedly, the synthesized ceria depending on calcination and treatments, the formation of Ce^{3+} and oxygen vacancies are anticipated. However, our XPS and EPR show no progressive increase in Ce^{3+} concentration for ceria samples of different sizes under *identical* preparation and heat treatment where change in lattice constant is recorded. The TPR also shows the constant reducible [O] content until below 5.3nm where extra oxygen in form of O_2^- is arisen. We therefore attribute the lattice expansion to the strain due to increasing surface energy.